



Geophysical Research Letters

RESEARCH LETTER

10.1029/2020GL090411

Key Points:

- Dominant air mass transport and topographic characteristics influence the synchronization structure and propagation patterns of heatwaves
- Event Synchronization metrics can identify the source and sink regions primarily responsible for heatwave propagations
- Network coefficients able to capture the spatial dependency between warm-period heatwave events occurring at different locations

Supporting Information:

· Supporting Information S1

Correspondence to:

A. K. Mishra, ashokm@g.clemson.edu

Citation:

Mondal, S., & Mishra, A. K. (2021). Complex networks reveal heatwave patterns and propagations over the USA. *Geophysical Research Letters*, 48, e2020GL090411https://doi.org/10.1029/2020GL090411

Received 17 AUG 2020 Accepted 15 DEC 2020

© 2020. American Geophysical Union. All Rights Reserved.

Complex Networks Reveal Heatwave Patterns and Propagations Over the USA

Somnath Mondal¹ and Ashok Kumar Mishra¹

¹Glenn Department of Civil Engineering, Clemson University, Clemson, SC, USA

Abstract Quantifying the dynamical linkage, co-evolution, and propagation of regional heatwaves is essential to minimize socio-economic losses. Here, we investigate such network structure and propagation characteristics for warm period (May–September) heatwaves over Conterminous United States using a complex network approach based on daily maximum temperature. The concept of Event Synchronization (ES) is applied to identify the source and sink regions primarily responsible for heatwave propagations and the strength of association between these regions. The network coefficients are derived to evaluate the extremal dependence, co-evolution, and spatial propagation of large scale heatwave events. The topology and propagation of heatwaves are influenced by the spatial distribution of the zonal and meridional air mass transport. Furthermore, we demonstrated the application of ES metrics and the network coefficients for heatwave days prediction between source and sink regions with true positive rate of 63% at a lead time of 2 days.

Plain Language Summary The large scale heatwave events have become very common over the Conterminous United States. The examples include heatwave events in Chicago and the Gulf coastal plains (2019 and 2020) and the recent ongoing extreme heat event in California (August 2020). The United States incurs significant socio-economic losses and health problems due to exposure to heatwaves. Under climate change, such heatwaves are likely to increase in different parts of the world, leading to increased socio-economic impacts. We apply complex network analysis to understand the USA heatwaves' regional connectivity and the underlying physical mechanisms. The derived information is essential in the forecasting of heatwaves.

1. Introduction

Climate change and seasonal variability have increased extreme events (e.g., drought and heatwave) in a warming world (Konapala et al., 2020; Mukherjee & Mishra, 2020). Major heatwave (HW) events have caused a significant socio-economic loss (Horton et al., 2016) in different regions around the world, such as Europe (2003), Russia (2010), South Asia and Middle East (2015), Southeast Asia (2016), and the recent HW in Chicago, USA (2019). Besides, HW immensely contributes to the increased mortality and morbidity (Anderson & Bell, 2009; Fuhrmann et al., 2016; Gasparrini et al., 2015), wildfire events (Shaposhnikov et al., 2014), loss in crop yield (Wegren, 2011) and infrastructure damage (García-Herrera et al., 2010) along with several other adverse effects (Battisti & Naylor, 2009; Schlenker & Roberts, 2009). Nonetheless, current mean global-scale warming is highly likely to amplify heatwave characteristics, such as magnitude, frequency, and duration (Coumou & Robinson, 2013; Coumou et al., 2013; Horton et al., 2016).

Multiple studies have investigated the USA's heatwave characteristics (Smith et al., 2013), prediction (McKinnon et al., 2016), climatology in the context of past, present, and future scenarios (Chapman et al., 2019; Grotjahn & Huynh, 2018; Lyon & Barnston, 2017; Schoof et al., 2017; Vogel et al., 2020; Wobus et al., 2018), spatial variability (Deng et al., 2018; Keellings & Moradkhani, 2020) along with attribution studies (Chiriaco et al., 2014; Durre et al., 2000; Liao et al., 2018; Lorenz et al., 2010; Zhao et al., 2019). However, to the best of our knowledge, no prior studies investigated spatial dependency (or synchronization) and propagation of heatwaves and their associated mechanisms. Explicit knowledge of such spatial relationships shared by heatwaves is crucial for better estimation of predictability and high-end risks imposed by such extreme events (Horton et al., 2016).

MONDAL AND MISHRA 1 of 12



Recently, the complex structure of climate systems are investigated by implementing the CN based algorithms (Boers et al., 2013; Konapala & Mishra, 2017; Malik et al., 2012; Mondal et al., 2020); for example, analysis of extreme summer precipitation (Boers et al., 2013; Mondal et al., 2020), and drought events over USA (Konapala et al., 2017). In this study, the concept of CN coefficients and event synchronization algorithms are applied to investigate extremal dependence, co-evolution, and spatial propagation of HW events. The objectives of this study are: (a) to map the topology of synchronization (dynamical similarity), spatial distribution, and propagation of HWs over the Conterminous United States (CONUS), (b) to identify the source and sink regions that control heatwave propagation, and (c) to illustrate the applications of CN metrics to quantify the direction of propagation and prediction of heatwaves.

2. Data

The CPC Global Unified Gauge-Based Analysis of daily maximum temperature (T-max) data (Sun et al., 2018) for 1979–2018, provided by the NOAA/OAR/ESRL PSD, USA at a spatial resolution of 0.5° x 0.5° is used in this study. The CPC data have key advantages, such as it displays less bias in representing extreme values compared to the Parameter-elevation Regressions on Independent Slopes Model (PRISM) data set (Behnke et al., 2016), and it has higher station density over CONUS (Sun et al., 2018). Additional variables, such as 1,000 and 500 mb geopotential height, zonal, and meridional wind components were obtained from the NCEP/NCAR Reanalysis 1 data (Kalnay et al., 1996).

3. Methodology

3.1. Heatwave Events

Multiple HW definitions exist in the literature; however, they all represent a continuous period of elevated temperature (Perkins, 2015). This study defines heatwave for each grid-location as a period (≥3 consecutive days) when the daily maximum temperature exceeds calendar day 90th percentile during the warm periods of the considered years 1979–2018. The 90th percentile is calculated based on the daily maximum temperature, centered on a 15-day window (Schoof et al., 2017). In this study, we selected a relative threshold (Alexander et al., 2006; Perkins et al., 2012) instead of an absolute threshold to preserve physical extremes of locations having completely different climatological settings. We selected a minimum number of three consecutive hot days to define a heatwave event (Meehl & Tebaldi, 2004; Russo et al., 2014).

3.2. Event Synchronization Approach and Complex Network Analysis

The event synchronization (ES, Quiroga et al., 2002) measures the magnitude of synchronization by counting the number of temporally coinciding HWs after allowing a possibility of a dynamic delay between any two grid locations i and j. The concept of ES can quantify the space-time dynamics of extreme natural events by coupling the lagged occurrence of extreme events at different locations. The concept of ES has previously been applied in climate-extreme related researches, such as extreme precipitation events (Boers et al., 2013; Mondal et al., 2020), drought propagation (Konapala & Mishra, 2017), and streamflow analysis (Sivakumar & Woldemeskel, 2014).

In the present study, the synchronization and delay (Table S1) values for all pairs of grid points are calculated using ES metric (Quian Quiroga et al., 2002) by selecting only 5% of the strongest values (of high statistical significance; Text S1) to form the connections between grid points. Two different types of complex networks (undirected and directed) were derived based on the synchronization and delay matrix by considering that every grid point act as a vertex of the complex network. At the same time, the connections between them represent the edges (Mondal et al., 2020). An undirected CN consists of all the vertices and pairwise relationships where each connection signifies synchronization in HW occurrences between the two connected grid-locations without presuming any sense of direction. A directed CN comprises connections among the grid-locations where every relationship is based on the delayed time occurrence (or delay) among the connected nodes. The direction is significant to capture the spatial propagation of HWs along with the underlying driver meteorological processes.

MONDAL AND MISHRA 2 of 12

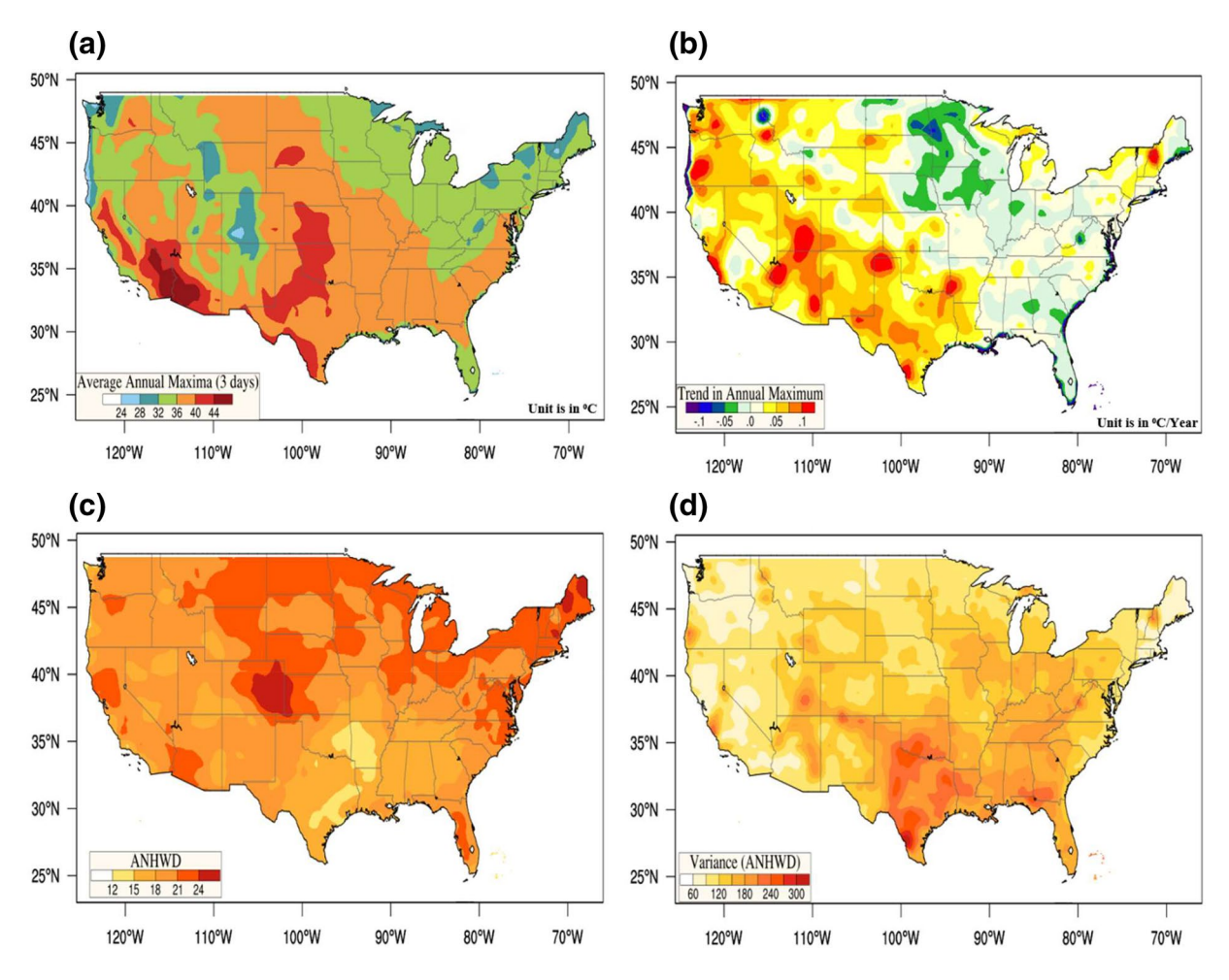


Figure 1. Warm-time (May-September): (a) 3-day moving average of annual maximum temperature (3d-AMT), (b) trends associated with the 3d-AMT, (c) the average number of heatwave days (ANHWD), and (d) Variance of ANHWD or Interannual variability of heatwave days for the period of 1979–2018.

Based on the undirected CN, four network coefficients were derived, namely degree centrality (DC), betweenness centrality (BC), clustering coefficient (CC), and mean synchronized distance (MSD). Similarly, from the directed CN, we derive three network coefficients: network divergence (ND), inward orientation, and outward orientation. The detailed illustration of ES, the complex network methodology, the definitions, and the derivation of network coefficients provided in Text S1. A concise and brief description of the network coefficients (Mondal et al., 2020) is presented in Table S1. The finite spatial embedding approach generally applied for boundary connections are discussed in Text S2, and the spatial plots for the network coefficients corresponding to boundary connection are provided in Figures S1–S3.

4. Results

4.1. Overview of Heatwave in CONUS

We provide the spatial distribution of the long-term mean (1979–2018) of a 3-day moving average of annual maximum temperature (3d-AMT) to determine the likelihood of possible maximum annual extreme events over CONUS. The 3d-AMT varies from 20° C to 48° in the southwest (Figure 1a). The decreasing tendency of temperature with increasing latitude is prominent, although the Northern Great Plains and Midwest region display high values (>36°C), indicating possible amplification of temperature extremes in these regions. The atmospheric humidity plays a distinctive role in the spatial variability of extreme temperature through partitioning downward solar radiation into sensible heat. Such behavior results in more amplification of day-time temperature in the arid southwest than humid Southeast, although both are in the same latitude.

MONDAL AND MISHRA 3 of 12



Furthermore, in transitional climate regions (e.g., Texas and California), the soil-temperature coupling can play a decisive role in day time temperature amplification (Miralles et al., 2012; Seneviratne et al., 2010).

We investigated the trends associated with the 3d-AMT (Figure 1b) for grid-locations over CONUS using Sen's Slope method (Perkins et al., 2012; Sen, 1968). Overall, positive trends (>0.09 Celsius/Year) are observed over CONUS with comparatively higher values clustered around the geographical regions located from West of Texas to Southern California, Oregon, and Washington. Few regions located in the Midwest and Southeast display negative trends (<-0.04 Celsius/Year). The negative trend in temperature extremes in the Southeast has been reported in previous studies (Alexander et al., 2006; Coumou et al., 2013), often known as "Warming hole."

The average number of heatwave days (ANHWD) over the CONUS varies from 10 to 28 days (Figure 1c) during the warm period. Heatwave days are comparatively more frequent in the northern half of the CONUS. However, a higher number of heatwave days (>20 days) can be observed over the west coast of California, Southwest, and southwest Florida. Similar high ANHWD can be observed near Michigan Lake and far northeastern regions of the CONUS. The low values of ANHWD can be observed in the regions located in South-Central parts of CONUS extending from the South of Texas. The possible reason for a smaller number of ANHWD is due to the higher temperature thresholds for defining the heatwave event and higher interannual variability between the number of heatwave days between 1979 and 2018 (Figure 1d). Due to the highest interannual variability, the number of heatwave days can substantially increase in a particular year over these regions. It is probably due to summer heatwaves' strong dependence on soil-temperature coupling observed in this region (E. Lee et al., 2016; Miralles et al., 2012). The detailed definition of 3-d AMT and ANHWD is present in Table S2.

Clearly, the spatial patterns of temperature extremes (heatwaves) evolve in clusters. We investigated the spatial association among heatwaves over CONUS using complex network analysis in the following section.

4.2. Complex Network Analysis of Heatwave

4.2.1. Degree Centrality

In Network Science, the DC signifies the number of grid-points displaying synchrony corresponding to an event's occurrence with respect to a given node (Mondal et al., 2020). In this study, the DC of a grid-location indicates the number of its neighbors experiencing simultaneous HW occurrences within the maximum time lag of 3 days. Previous network studies have found that a high degree (Olivares et al., 2013; Pazouki et al., 2014) nodes may act as "hub or supernode" (Tsonis et al., 2006). In terms of climate science, such hubs can be responsible for teleconnections and large-scale communication, which are critical for any complex network structure and dynamics (Pei & Makse, 2013).

Most of the higher DC grids are concentrated on the northern half of the CONUS (Figure 2a). Highest DCs are observed near Michigan Lake and the Northwest part of CONUS, whereas the lowest DCs are concentrated near the coastal region of CONUS. Heatwaves in the coastal zone are extremely localized and may be poorly associated with underlying physical linkages in the inland heatwaves. This may be feasible as inland thermal low may limit the sea-land breeze to travel far distant into the interior land regions (Y. Y. Lee & Grotjahn, 2016). However, the westerly wave fluxes and the dominant subsidence condition may lead to sustained heating and horizontal advection of heat (Y. Y. Lee & Grotjahn, 2016) in the coastal regions in the western United States. This may lead to the propagation of heatwaves to a large extent of inland areas. Detection of such influence can be confirmed if such regions also display low CC and high BC. Previous climate-network studies (Donges et al., 2009b) have termed such locations with low DC and high BC as "Bottleneck of energy flow."

The spatial connection between regional heatwaves can be explained by dominant meteorological variables associated with regional DCs. For example, the higher DC in the midlatitude can be explained by its tendency to experience the meandering of the westerly jet stream, which splits upper-level atmospheric winds (Pfahl & Wernli, 2012). This forces the downwind region blocked from the zonal jet stream flow (Pezza et al., 2012). Such a semi-stationary pressure ridge can substantially decrease local weather variability and

MONDAL AND MISHRA 4 of 12

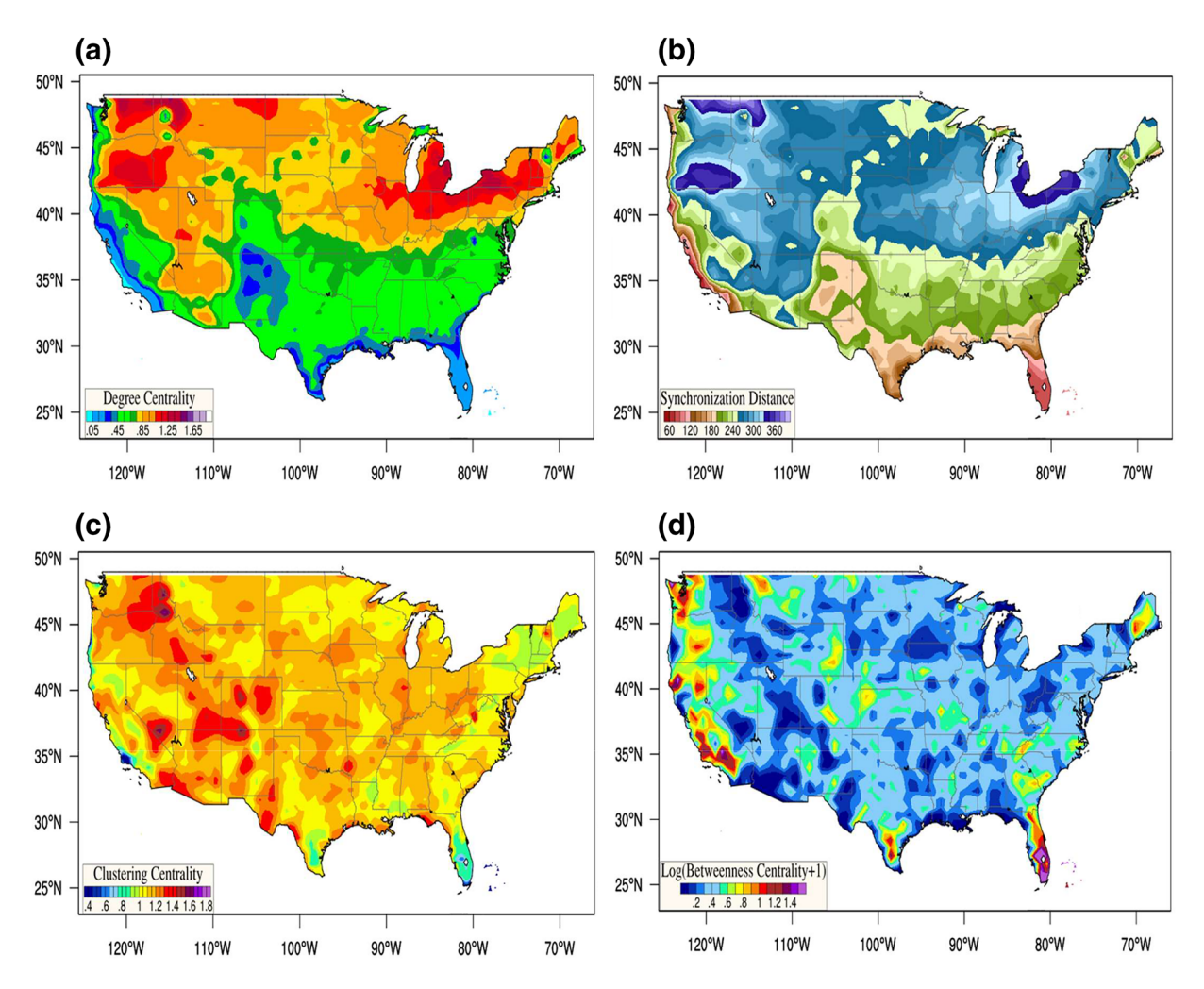


Figure 2. (a) Degree Centrality (DC), (b) Mean Synchronization Distance (MSD) (in km), (c) Clustering Coefficient (CC), and (d) Betweenness Centrality (BC). These network coefficients are derived based on the undirected complex network.

provide ample time for heatwaves to build up over a vast region (Meehl & Tebaldi, 2004). Similarly, the heatwaves in the southern half of CONUS can be attributed to warm-period continental-wards oscillatory movement of the subtropical ridge over the Atlantic and Pacific along with the progression of the Warm-period (Figure S4), termed as "persistent highs" (Marshall et al., 2014), which is typically located 5°–10° equatorward from the location of blocking highs (Perkins, 2015). To ascertain the physical mechanism associated with different DC values over CONUS, we first choose two different grid-location with very high and low DC (Figures S5a–S5b). We further calculate 500 mb geopotential height and zonal wind anomaly corresponding to the days when each grid location is synchronized with more than 90% of its connections (Text S1). We observe that corresponding to the high DC location (Figure S5a) there is a prominent high-pressure anomaly over the same region (Figure S5e) blocking zonal airstream over western half of CONUS (Figure S5f). The high-pressure anomaly is much weakened in the case of the low DC (Figure S5b) location and is present mainly over California (Figure S5g). Furthermore, the 500 mb zonal air mass transport in the midlatitude is not blocked (Figure S5h), with its negative anomaly mostly centers over the considered grid-location.

4.2.2. Mean Synchronized Distance

The spatial distributions of the synchronization-scale of heatwaves over CONUS are quantified based on the MSD (Figure 2b). The synchronization scale refers to the distance beyond which a grid point does not

MONDAL AND MISHRA 5 of 12



display any significant synchronization in the occurrences of heatwaves. In other words, the MSD of any grid-location implies the average spatial scale of heatwave occurrences.

The distribution of MSD is spatially correlated with the degree centrality (Figure S6), and the higher values are mostly located in the northern half of CONUS. The higher values of MSD observed over the Northern part of CONUS often result in more significant spatial scale events. This further validates the influence of blocking high on the heatwaves over this region (Meehl & Tebaldi, 2004; Pfahl & Wernli, 2012). Similar to DC, the highest values of MSD are positioned surrounding Michigan Lake and in the Northwest region. These regions may act as clusters of hubs or supernodes (Konapala & Mishra, 2017; Tsonis & Roebber, 2004; Tsonis et al., 2006) such that heatwave conditions over these regions may render a large area of CONUS vulnerable to heatwaves. One can attribute the higher mortality rate in the Midwest region (Anderson & Bell, 2011; Whitman et al., 1997) to this combination of large spatial scale and high peak amplitude of heatwaves (Figure S7).

4.2.3. Clustering Coefficient and Betweenness Centrality

The CC captures the extent of interconnectivity among the neighbors connected to the node (Mondal et al., 2020). It can be interpreted as the heatwaves occurring in the regions with a higher magnitude of CC are more likely to be spatially connected to its immediate neighbors and would seldom propagate to farther areas. On the other hand, BC represents the amount of information propagating through a specific node of a CN system. The importance of a node (i.e., geographical location) within the global topology of the CN system can be determined based on the magnitude of the BC (Donges et al., 2009a).

The strongest CC and the lowest BC values can be observed over North American Cordillera's high altitude areas (Figures2c and d). It indicates the presence of extremely localized heatwaves (high CC) in the high mountain ranges of the Rockies, Cascade, and the Sierra Nevada, which synchronize less with distant neighbors (low BC and lesser MSD in comparison to its adjacent areas). On the other hand, high BC and low CC values can be observed over the West coast, especially at three sites: West of Washington, Northwest, and Southwest of California. In the previous studies, the latter two locations have been observed to propagate heatwaves into many inland regions of the western USA, such as California Central valley (Y. Y. Lee & Grotjahn, 2016). In contrast, the Northwest's heatwaves primarily emerge from the Northeastern flank of the Pacific ridge positioned at the west and Northwest of Washington during the warm period (Figure S4). Interestingly, these locations also display low DC indicating a large amount of heatwave propagation through a few linkages, often known as the bottleneck of energy flow (Donges et al., 2009a).

4.2.4. Propagation Characteristics of Heatwaves over CONUS

The inward and outward strength (Table S1) of each grid-location are calculated, and the difference between the inward and outward strength is used to derive Network Divergence (ND). A region with high positive (negative) values of ND represents the source (sink) of heatwave propagation. Figure 3a describes the network divergence of heatwaves over CONUS. Negative ND values are observed over the Northern Great Plains, extending from west of Wisconsin to the west coast. Higher magnitude negative ND values are mainly located over Montana, North Dakota, and in the coastal region of Oregon and California. Whereas positive ND values are mostly observed in the Midwest and Northeast with the highest magnitude are present in the southwest of Michigan Lake and Northeast. Overall, the positive ND gradient from west to east indicates a more substantial influence of eastwards zonal airflow on heatwave propagation over CONUS.

The directions of heatwave propagation are investigated based on the inward and outward orientation (Figures 3b–3c). The inward and outward strength for each grid is provided in the background to characterize and visualize the divergence and convergence of heatwaves. It can be observed that the western parts of CONUS likely to receive heatwaves from the coast. Strong heatwave divergence characteristics can be found in the coastal regions of California and Oregon (Figure 3b). Two coastal areas located in the Northwest and Southwest likely to propagate heatwaves into California (Figure 3c). This is consistent with two different sources of heat flow into the California central valley as noted in previous studies (Y. Y. Lee & Grotjahn, 2016). This further validates the likelihood of heatwave propagation through a small region and its

MONDAL AND MISHRA 6 of 12

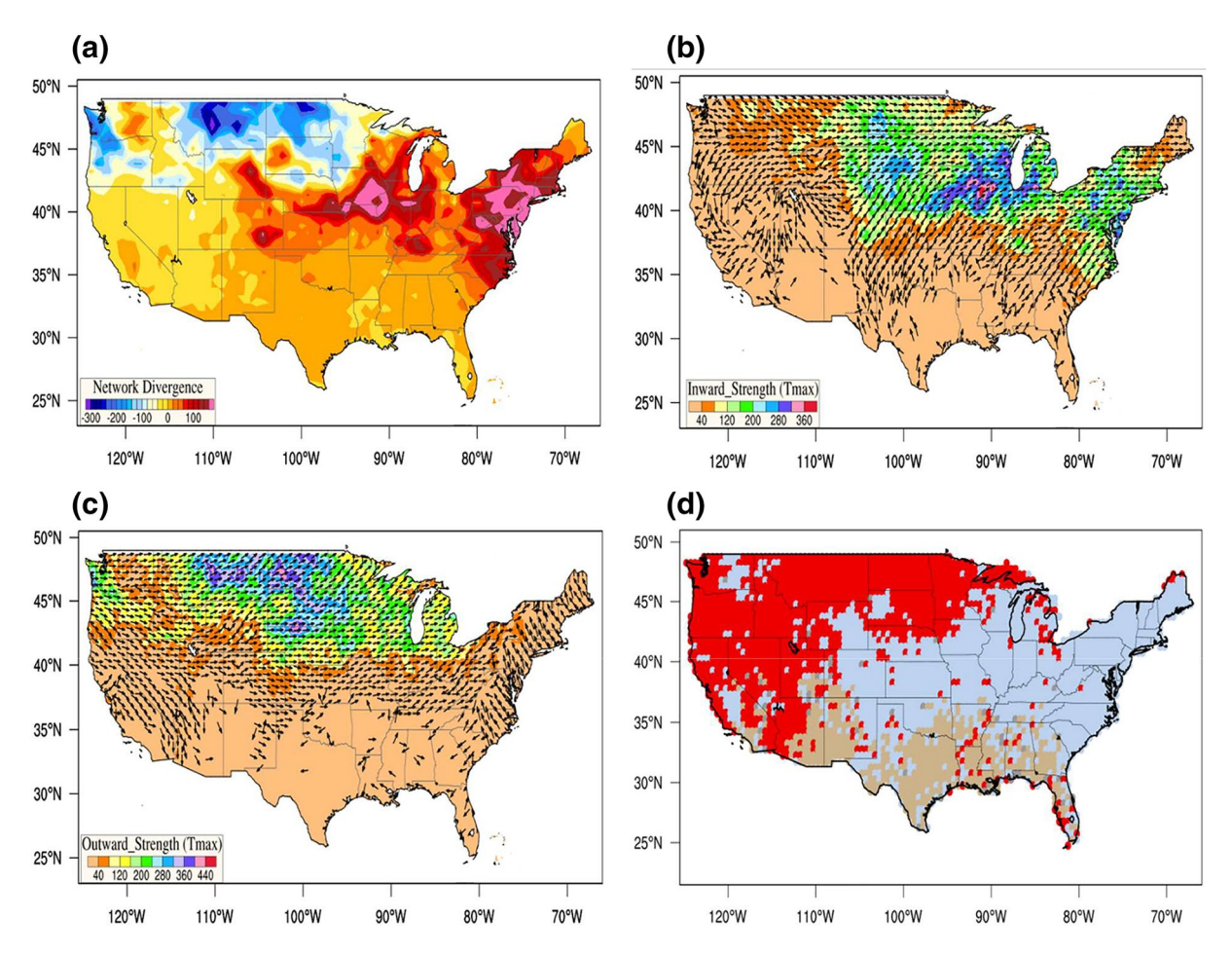


Figure 3. (a) Network Divergence, (b) Inward Orientation, (c) Outward Orientation, and (d) Spatial distribution of source and sink nodes of heatwaves. The red dots indicate source nodes (indegree < outdegree), whereas the light steel blue dots indicate sink nodes (indegree > outdegree). The dots in antique white color indicates isolated nodes with no indegree and outdegree. The three network coefficients (a–c) are derived based on the directed complex network.

divergence into a broader inland region due to the characteristics of low DC, low CC, and high BC. Similar divergence characteristics can be observed over Florida and Wyoming (Figure 3c).

The physical settings of air-mass transport over CONUS are further explored based on the climatology of surface velocity at 1,000 mb (Figure S8a) and the zonal strength of propagation of air (Figure S8b) by dividing the zonal component with the meridional component. Interestingly, regions with high outdegrees (Figure 3c) are dominated by air mass transport's high zonal strength. In contrast, both meridional and zonal air transport contributes to heatwaves over locations with high in-degree (Figure 3b). Low zonal strength can be observed in two regions. The first one is located over the east of the Rockies and extended from South Texas to the Northern Great Plains. The second one is over the west of the Rockies, which predominantly exists over Southwest USA. The areal extent of these two zones is potentially influenced by the North American Cordillera as the high altitude in north-south orientation blocks or disrupts air's zonal transport. Although the meridional component of air is generally lesser than the zonal component, such topographic blocking may force a zonal wind to be explicitly meridional (i.e., GPLLJ), resulting in comparatively lower propagation (Figure 3d) of heatwaves over Texas and Oklahoma.

4.2.5. Heatwave Propagation at Specific Locations

The individual grid can behave as a source or sink (Figure 3d) for heatwave propagation. The cluster of homogenous grids with high outward strength (i.e., source region) can form regional hubs that can propagate

MONDAL AND MISHRA 7 of 12

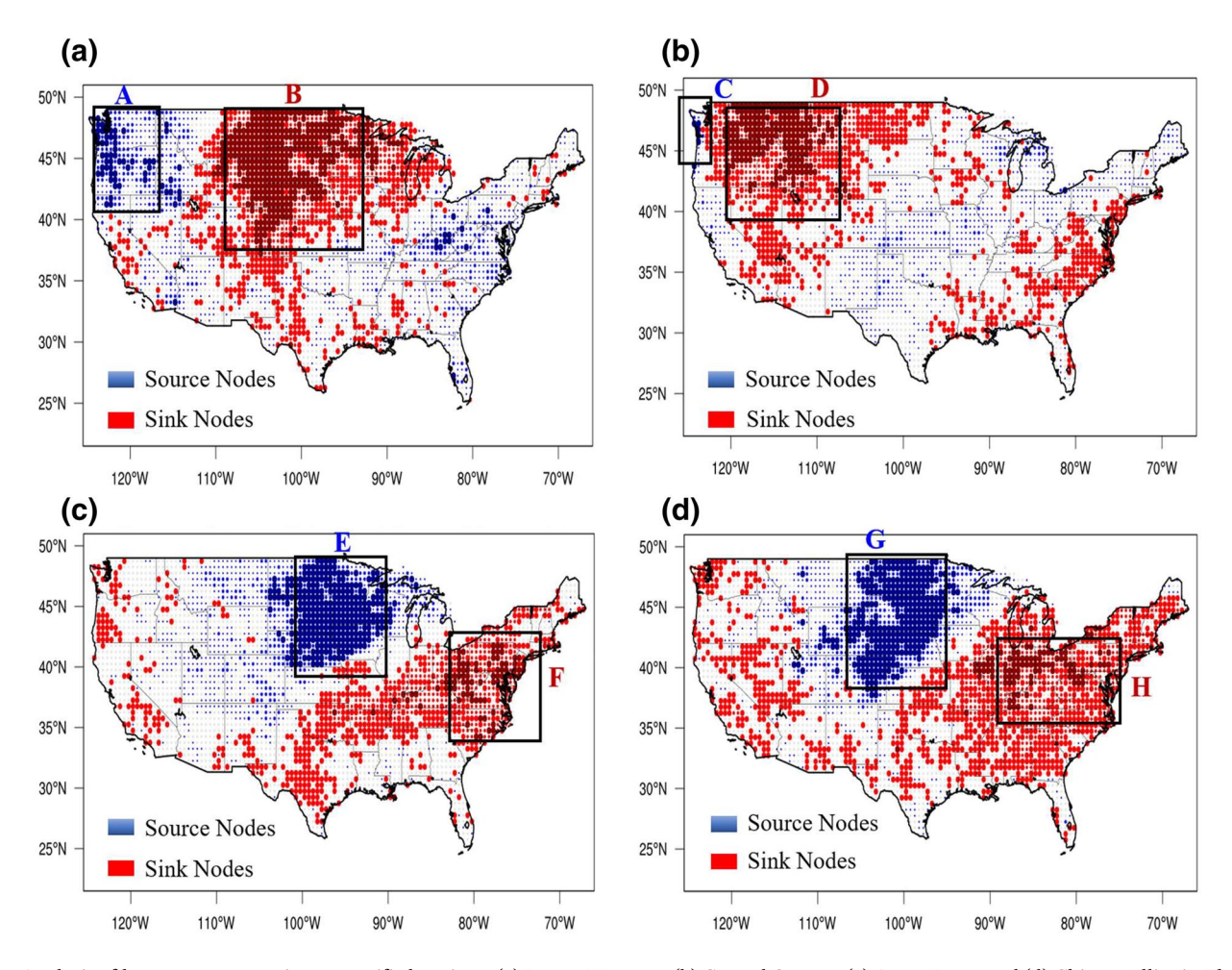


Figure 4. Analysis of heatwave propagation at specific locations: (a) Loma, Montana, (b) Coastal Oregon, (c) Ames, Iowa, and (d) Chicago, Illinois. The clusters of blue and red colors indicate source and sink regions for heatwave propagations.

heatwaves to different locations. Similarly, a cluster of homogenous grids with high inward strength (i.e., sink region) are vulnerable to heatwaves occurring at various locations. For illustration purposes, we selected four grid-locations to explain the potential application of source and sink regions for heatwave propagation (Figures 4a–4d).

We observe that heatwaves occur in the western part of Washington, Oregon, and Northwest California (Box A, Figure 4a), likely to propagate to Loma, Montana, which may further move eastward to the regions extending from the north of North Dakota to the south of Colorado (Box B, Figure 4a). To cross-check, we selected a spatial domain located over the West of Oregon. It can be observed that the heatwaves originate from the Pacific Northwest (Box C, Figure 4b) propagate to western Oregon, Eastern Washington, Idaho, and Montana (Box D, Figure 4b). This can be attributed to the air mass flowing from the direction of Northwest USA can propagate heatwaves to Montana (Wang et al., 2019) and further propagate eastward overland to a large extent.

Chicago (Illinois) witnessed the famous 1995s heatwave (Karl & Knight, 1997). We observe that heatwaves initiated over the Great Plains (Box E, Figure 4c) likely to proceed toward Chicago within three days. Heatwaves over Chicago may further migrate toward Pennsylvania and West Virginia (Box F, Figure 4c). Interestingly, the heatwaves initiated between 35.5°N to 49.5°N (Box G, Figure 4d) converge to Iowa, then further migrates to regions surrounding and east of Chicago (Box H, Figure 4d). This may be due to the potential influence of (southerly) meridional and (westerly) zonal air mass transport of heat that results in the convergence of heatwaves over the regions surrounding Chicago (Positive ND).

MONDAL AND MISHRA 8 of 12



4.2.6. Application of Network Metrics for Heatwave Predictions

We investigate the potential of ES metrics (Synchronization and Delay) and directed network coefficients (Network Divergence) to predict heatwave days at selected regions over CONUS. For illustration, we identify a source region (spatial extent of $2^{\circ} \times 2^{\circ}$, Figure S9a) located near to Loma, Montana, which propagates heatwaves to several other locations (Negative ND). The high value of regional outdegree (Text S1) corresponding to the source region indicates the most probable areas to experience heatwave after such an event occurs at the source region 1–3 days ahead (Figure S9b). We selected a lead time of 2 days to predict heatwave days from source to sink region. We formulate a new ES metric "syncd delay" (Text S3) by multiplying synchronization and delay (at a fixed time lag of 2 days) of each grid location over CONUS with respect to the source box (Text S3). The sink region (spatial extent of $2^{\circ} \times 2^{\circ}$) was selected over the areas situated at the junction of North and South Dakota (Figure S9a). This region displays high regional outdegree (Figure S9b) and increased positive syncd delay (Figure S9c) with respect to the source region, indicating heatwave propagations from the source to sink box. To visualize, we further constructed propagation direction based on three different boxes (Figure S9a) and a heatmap (Figure S9d) that clearly outlines many heatwave event (Text S3) propagations between source and sink boxes at a lag time of 2 days.

Once heatwave propagation between the source and sink boxes is ascertained, we selected time series of 100% spatially synchronized heatwave days (Text S3) over the source box as input. The desired output is the 2 day lagged time series of 100% spatially synchronized heatwave days over the sink box. We perform the prediction using a binary classification framework since the occurrence or nonoccurrence of heatwave days is distinct as two separate classes. The commonly used Linear Discriminant Analysis (LDA) classification algorithm (Balakrishnama et al., 1999; Mahdianpari et al., 2018) was used to develop a prediction model. A brief illustration of the LDA algorithm is provided in Text S3. The model performance was validated using metrics such as the Confusion matrix and the ROC curve, which indicates satisfactory performance with 63% accurate detection of heatwave days at the sink region in a lead time of 2 days (FiguresS11a and S11b). The satisfactory prediction performance can be attributed to the high lagged synchronization between the input and output grid-locations. The prediction accuracy can be further improved by incorporating additional variables such as sea surface temperature, high-level zonal, and meridional wind anomaly, which is known to influence triggering or evolution of heatwave event.

5. Conclusion

The study employs complex network analysis to investigate the topology, co-evolution, and spatial propagation of heatwaves over CONUS. The current research reveals the spatial patterns of heatwaves and their association with air mass transport distribution and the topography. The CN analysis reveals the heatwaves occurring in large parts of the western USA typically originate from California and Oregon's coastal areas. These specific coastal regions experience strong air subsidence conditions, which lead to the initiation of heatwaves (Y. Y. Lee & Grotjahn, 2016). We observed the lesser propagation strength of heatwaves over Texas and Oklahoma; this may be attributed to the North-south orientation of the North American Cordillera suppressing zonal air mass transport over Texas and Oklahoma. Most importantly, the combination of event synchronization metric and network coefficients has been able to identify heatwave propagation between regions, primarily acting as source or sink of heatwaves.

Nonetheless, the current study has a few limitations, such as a fixed value of maximum lag time (here 3 days) between the propagation of heatwave events. Additional source and sink regions can be identified, especially over the southern part of CONUS, by increasing the lag time. This aspect can be investigated in future studies to determine the potential influence of multiscale lag time on the propagation of heatwaves. The data length can be a key limitation for complex network analysis of extreme events (especially for drought-related studies). The extreme events collected over a more extended period can provide a reliable estimation of synchronization and heatwave's propagation over CONUS. Furthermore, the presence of substructures due to the effect of local-scale weather patterns are not explored in this study, which deserves special attention. Overall, the information obtained from the event synchronization metric and Network coefficients can be useful for developing an appropriate process or structure-based heatwave forecasting models.

MONDAL AND MISHRA 9 of 12



Data Availability Statement

The daily temperature data can be obtained from the NOAA/OAR/ESRL PSD, USA (https://psl.noaa.gov/data/gridded/data.cpc.globaltemp.html). Additional weather variables (Geopotential Height and wind) are obtained from NCEP/NCAR Reanalysis 1 (https://psl.noaa.gov/data/gridded/data.ncep.reanalysis.pressure.html).

Acknowledgments

AM is supported by the US National Science Foundation (NSF) Awards 1653841.

References

- Alexander, L. V., Zhang, X., Peterson, T. C., Caesar, J., Gleason, B., Tank, A. M. G. K., et al. (2006). Global observed changes in daily climate extremes of temperature and precipitation. *Journal of Geophysical Research*, 111(D5), D05109. https://doi.org/10.1029/2005JD006290
- Anderson, B. G., & Bell, M. L. (2009). Weather-related mortality: how heat, cold, and heat waves affect mortality in the United States. Epidemiology, 20(2), 205–213. https://doi.org/10.1097/EDE.0b013e318190ee08
- Anderson, G. B., & Bell, M. L. (2011). Heat waves in the United States: mortality risk during heat waves and effect modification by heat wave characteristics in 43 U.S. communities. *Environmental Health Perspectives*, 119(2), 210–218. https://doi.org/10.1289/ehp.1002313
- Balakrishnama, S., Ganapathiraju, A., & Picone, J. (1999). Linear discriminant analysis for signal processing problems. In *Proceedings IEEE Southeastcon'99*. Technology on the Brink of 2000 (Cat. No.99CH36300) (pp. 78–81). IEEE. 10.1109/SECON.1999.766096
- Battisti, D. S., & Naylor, R. L. (2009). Historical warnings of future food insecurity with unprecedented seasonal heat. *Science*, 323(5911), 240–244. https://doi.org/10.1126/science.1164363
- Behnke, R., Vavrus, S., Allstadt, A., Albright, T., Thogmartin, W. E., & Radeloff, V. C. (2016). Evaluation of downscaled, gridded climate data for the conterminous United States. *Ecological Applications*, 26(5), 1338–1351. https://doi.org/10.1002/15-1061
- Boers, N., Bookhagen, B., Marwan, N., Kurths, J., & Marengo, J. (2013). Complex networks identify spatial patterns of extreme rainfall events of the South American Monsoon System. *Geophysical Research Letters*, 40(16), 4386–4392. https://doi.org/10.1002/grl.50681
- Chapman, S. C., Watkins, N. W., & Stainforth, D. A. (2019). Warming Trends in Summer Heatwaves. *Geophysical Research Letters*, 46(3), 1634–1640. https://doi.org/10.1029/2018GL081004
- Chiriaco, M., Bastin, S., Yiou, P., Haeffelin, M., Dupont, J.-C., & Stéfanon, M. (2014). European heatwave in July 2006: Observations and modeling showing how local processes amplify conducive large-scale conditions. *Geophysical Research Letters*, 41(15), 5644–5652. https://doi.org/10.1002/2014GL060205
- Coumou, D., Robinson, A., & Rahmstorf, S. (2013). Global increase in record-breaking monthly-mean temperatures. Climatic Change, 118(3), 771–782. https://doi.org/10.1007/s10584-012-0668-1
- Deng, K., Yang, S., Ting, M., Lin, A., & Wang, Z. (2018). An Intensified mode of variability modulating the summer heat waves in Eastern Europe and Northern China. *Geophysical Research Letters*, 45(20), 11361–11369. https://doi.org/10.1029/2018GL079836
- Donges, J. F., Zou, Y., Marwan, N., & Kurths, J. (2009). Complex networks in climate dynamics. *The European Physical Journal: Special Topics*, 174(1), 157–179. https://doi.org/10.1140/epjst/e2009-01098-2
- Donges, J. F., Zou, Y., Marwan, N., & Kurths, J. (2009). The backbone of the climate network. EPL (Europhysics Letters), 87(4), 48007. https://doi.org/10.1209/0295-5075/87/48007
- Durre, I., Wallace, J. M., & Lettenmaier, D. P. (2000). Dependence of extreme daily maximum temperatures on antecedent soil moisture in the contiguous United States during summer. *Journal of Climate*, 13(14), 2641–2651. https://doi.org/10.1175/1520-0442(2000)013<2641:DOEDMT>2.0.CO;2
- Fuhrmann, C. M., Sugg, M. M., Konrad, C. E., & Waller, A. (2016). Impact of extreme heat events on emergency department visits in North Carolina (2007-2011). *Journal of Community Health*, 41(1), 146–156. https://doi.org/10.1007/s10900-015-0080-7
- García-Herrera, R., Díaz, J., Trigo, R. M., Luterbacher, J., & Fischer, E. M. (2010). A review of the European summer heat wave of 2003. Critical Reviews in Environmental Science and Technology, 40(4), 267–306. https://doi.org/10.1080/10643380802238137
- Gasparrini, A., Guo, Y., Hashizume, M., Lavigne, E., Zanobetti, A., Schwartz, J., et al. (2015). Mortality risk attributable to high and low ambient temperature: A multicountry observational study. *The Lancet*, 386(9991), 369–375. https://doi.org/10.1016/S0140-6736(14)62114-0
- Grotjahn, R., & Huynh, J. (2018). Contiguous US summer maximum temperature and heat stress trends in CRU and NOAA Climate Division data plus comparisons to reanalyzes. *Scientific Reports*, 8, 11146. https://doi.org/10.1038/s41598-018-29286-w
- Horton, R. M., Mankin, J. S., Lesk, C., Coffel, E., & Raymond, C. (2016). A review of recent advances in research on extreme heat events. Current Climate Change Reports, 2(4), 242–259. https://doi.org/10.1007/s40641-016-0042-x
- Kalnay, E., Kanamitsu, M., Kistler, R., Collins, W., Deaven, D., Gandin, L., et al. (1996). The NCEP/NCAR 40-year reanalysis project. Bulletin of the American Meteorological Society, 77(3), 437–472. https://doi.org/10.1175/1520-0477(1996)077<0437:TNYRP>2.0.CO;2
- Karl, T. R., & Knight, R. W.. (1997). The 1995 Chicago Heat Wave: How Likely Is a Recurrence? Bulletin of the American Meteorological Society, 78(6), 1107–1120. https://doi.org/10.1175/1520-0477(1997)078<1107:TCHWHL>2.0.CO;2
- Keellings, D., & Moradkhani, H. (2020). Spatiotemporal evolution of heat wave severity and coverage across the United States. Geophysical Research Letters, 47(9), e2020GL087097. https://doi.org/10.1029/2020GL087097
- Konapala, G., & Mishra, A. (2017). Review of complex networks application in hydroclimatic extremes with an implementation to characterize spatio-temporal drought propagation in continental USA. *Journal of Hydrology*, 555, 600–620. https://doi.org/10.1016/j. ihydrol.2017.10.033
- Konapala, G., Mishra, A. K., Wada, Y. et al. (2020) Climate change will affect global water availability through compounding changes in seasonal precipitation and evaporation. *Nature Communications* 11, 3044.
- Lee, E., Bieda, R., Shanmugasundaram, J., & Richter, H. B. (2016). Land surface and atmospheric conditions associated with heat waves over the Chickasaw Nation in the South Central United States. *Journal of Geophysical Research: Atmospheres*, 121(11), 6284–6298. https://doi.org/10.1002/2015JD024659
- Lee, Y.-Y., & Grotjahn, R. (2016). California Central Valley summer heat waves form two ways. *Journal of Climate*, 29(3), 1201–1217. https://doi.org/10.1175/JCLI-D-15-0270.1
- Liao, W., Liu, X., Li, D., Luo, M., Wang, D., Wang, S., et al. (2018). Stronger contributions of urbanization to heat wave trends in wet climates. Geophysical Research Letters, 45(20), 11310–11317. https://doi.org/10.1029/2018GL079679
- Lorenz, R., Jaeger, E. B., & Seneviratne, S. I. (2010). Persistence of heat waves and its link to soil moisture memory. *Geophysical Research Letters*, 37(9), L09703. https://doi.org/10.1029/2010GL042764

MONDAL AND MISHRA 10 of 12



- Lyon, B., & Barnston, A. G. (2017). Diverse characteristics of U.S. summer heat waves. Journal of Climate, 30(19), 7827–7845. https://doi.org/10.1175/JCLI-D-17-0098.1
- Mahdianpari, M., Salehi, B., Mohammadimanesh, F., Brisco, B., Mahdavi, S., Amani, M., & Granger, J. E. (2018). Fisher linear discriminant analysis of coherency matrix for wetland classification using PolSAR imagery. *Remote Sensing of Environment*, 206, 300–317. https://doi.org/10.1016/i.rse.2017.11.005
- Malik, N., Bookhagen, B., Marwan, N., & Kurths, J. (2012). Analysis of spatial and temporal extreme monsoonal rainfall over South Asia using complex networks. *Climate Dynamics*, 39(3), 971–987. https://doi.org/10.1007/s00382-011-1156-4
- Marshall, A. G., Hudson, D., Wheeler, M. C., Alves, O., Hendon, H. H., Pook, M. J., & Risbey, J. S. (2014). Intra-seasonal drivers of extreme heat over Australia in observations and POAMA-2. Climate Dynamics, 43(7), 1915–1937. https://doi.org/10.1007/s00382-013-2016-1
- McKinnon, K. A., Rhines, A., Tingley, M. P., & Huybers, P. (2016). Long-lead predictions of eastern United States hot days from Pacific sea surface temperatures. *Nature Geoscience*, 9(5), 389–394. https://doi.org/10.1038/ngeo2687
- Meehl, G. A., & Tebaldi, C. (2004). More intense, more frequent, and longer lasting heat waves in the 21st century. *Science*, 305(5686), 994–997. https://doi.org/10.1126/science.1098704
- Miralles, D. G., van den Berg, M. J., Teuling, A. J., & de Jeu, R. A. M. (2012). Soil moisture-temperature coupling: A multiscale observational analysis. *Geophysical Research Letters*, 39(21), L21707. https://doi.org/10.1029/2012GL053703
- Mondal, S., Mishra, A. K., & Leung, L. R. (2020). Spatiotemporal characteristics and propagation of summer extreme precipitation events over United States: A complex network analysis. *Geophysical Research Letters*, 47(15), e2020GL088185. https://doi.org/10.1029/2020GL088185
- Mukherjee, S., Mishra, A. K. (2020), Increase in compound drought and heatwaves in a Warming World, *Geophysical Research Letters*, 48(1), e2020GL090617. https://doi.org/10.1029/2020GL090617
- Olivares, T., Royo, F., & Ortiz, A. M. (2013). An experimental testbed for smart cities applications. In *Proceedings of the 11th ACM international symposium on mobility management and wireless access* (pp. 115–118). Barcelona, Spain: Association for Computing Machinery. https://doi.org/10.1145/2508222.2508243
- Pazouki, S., Haghifam, M.-R., & Moser, A. (2014). Uncertainty modeling in optimal operation of energy hub in presence of wind, storage and demand response. *International Journal of Electrical Power & Energy Systems*, 61, 335–345. https://doi.org/10.1016/j.ijepes.2014.03.038
- Pei, S., & Makse, H. A. (2013). Spreading dynamics in complex networks. *Journal of Statistical Mechanics: Theory and Experiment*, 2013(12), https://doi.org/10.1088/1742-5468/2013/12/P12002
- Perkins, S. E.. (2015). A review on the scientific understanding of heatwaves—Their measurement, driving mechanisms, and changes at the global scale. *Atmospheric Research*, 164–165, 242–267. https://doi.org/10.1016/j.atmosres.2015.05.014
- Perkins, S. E., Alexander, L. V., & Nairn, J. R. (2012). Increasing frequency, intensity and duration of observed global heatwaves and warm spells. Geophysical Research Letters, 39(20), L20714. https://doi.org/10.1029/2012GL053361
- Pezza, A. B., van Rensch, P., & Cai, W. (2012). Severe heat waves in Southern Australia: synoptic climatology and large scale connections. Climate Dynamics, 38(1), 209–224. https://doi.org/10.1007/s00382-011-1016-2
- Pfahl, S., & Wernli, H. (2012). Quantifying the relevance of atmospheric blocking for co-located temperature extremes in the Northern Hemisphere on (sub-)daily time scales. *Geophysical Research Letters*, 39(12), L12807. https://doi.org/10.1029/2012GL052261
- Quian Quiroga, R., Kreuz, T., & Grassberger, P. (2002). Event synchronization: a simple and fast method to measure synchronicity and time delay patterns. Physical Review. E, Statistical, Nonlinear, and Soft Matter Physics, 66(4 Pt 1), 041904. https://doi.org/10.1103/ PhysRevE.66.041904
- Russo, S., Dosio, A., Graversen, R. G., Sillmann, J., Carrao, H., Dunbar, M. B., et al. (2014). Magnitude of extreme heat waves in present climate and their projection in a warming world. *Journal of Geophysical Research: Atmospheres*, 119(22), 12500–12512. https://doi.org/10.1002/2014JD022098
- Schlenker, W., & Roberts, M. J. (2009). Nonlinear temperature effects indicate severe damages to U.S. crop yields under climate change. Proceedings of the National Academy of Sciences, 106(37), 15594–15598. https://doi.org/10.1073/pnas.0906865106
- Schoof, J. T., Ford, T. W., & Pryor, S. C. (2017). Recent changes in U.S. regional heat wave characteristics in observations and reanalyzes. Journal of Applied Meteorology and Climatology, 56(9), 2621–2636. https://doi.org/10.1175/JAMC-D-16-0393.1
- Sen, P. K. (1968). Estimates of the regression coefficient based on Kendall's Tau. *Journal of the American Statistical Association*, 63(324), 1379–1389. https://doi.org/10.2307/2285891
- Seneviratne, S. I., Corti, T., Davin, E. L., Hirschi, M., Jaeger, E. B., Lehner, I., et al. (2010). Investigating soil moisture-climate interactions in a changing climate: A review. *Earth-Science Reviews*, 99(3), 125–161. https://doi.org/10.1016/j.earscirev.2010.02.004
- Sivakumar, B., & Woldemeskel, F. M. (2014). Complex networks for streamflow dynamics. *Hydrology and Earth System Sciences*, 18(11), 4565–4578. https://doi.org/10.5194/hess-18-4565-2014
- Smith, T. T., Zaitchik, B. F., & Gohlke, J. M. (2013). Heat waves in the United States: Definitions, patterns and trends. Climatic Change, 118(3), 811–825. https://doi.org/10.1007/s10584-012-0659-2
- Sun, Q., Miao, C., Duan, Q., Ashouri, H., Sorooshian, S., & Hsu, K.-L. (2018). A review of global precipitation data sets: Data sources, estimation, and intercomparisons. *Reviews of Geophysics*, 56(1), 79–107. https://doi.org/10.1002/2017RG000574
- Tsonis, A. A., & Roebber, P. J. (2004). The architecture of the climate network. *Physica A: Statistical Mechanics and its Applications*, 333, 497–504. https://doi.org/10.1016/j.physa.2003.10.045
- Tsonis, A. A., Swanson, K. L., & Roebber, P. J. (2006). What Do Networks Have to Do with Climate? Bulletin of the American Meteorological Society, 87(5), 585–596. https://doi.org/10.1175/BAMS-87-5-585
- Vogel, M. M., Zscheischler, J., Fischer, E. M., & Seneviratne, S. I. (2020). Development of future heatwaves for different hazard thresholds. Journal of Geophysical Research: Atmospheres, 125(9), e2019JD032070. https://doi.org/10.1029/2019JD032070
- Wang, H., Schubert, S. D., Koster, R. D., & Chang, Y. (2019). Attribution of the 2017 Northern high plains drought. *Bulletin of the American Meteorological Society*, 100(1), S25–S29. https://doi.org/10.1175/BAMS-D-18-0115.1
- Wegren, S. K. (2011). Food security and Russia's 2010 drought. Eurasian Geography and Economics, 52(1), 140–156. https://doi. org/10.2747/1539-7216.52.1.140
- Whitman, S., Good, G., Donoghue, E. R., Benbow, N., Shou, W., & Mou, S. (1997). Mortality in Chicago attributed to the July 1995 heat wave. *American Journal of Public Health*, 87(9), 1515–1518. https://doi.org/10.2105/AJPH.87.9.1515

MONDAL AND MISHRA 11 of 12



10.1029/2020GL090411



Wobus, C., Zarakas, C., Malek, P., Sanderson, B., Crimmins, A., Kolian, M., et al. (2018). Reframing future risks of extreme heat in the

United States. *Earth's Future*, 6(9), 1323–1335. https://doi.org/10.1029/2018EF000943
Zhao, A., Bollasina, M. A., & Stevenson, D. S. (2019). Strong influence of aerosol reductions on future heatwaves. *Geophysical Research* Letters, 46(9), 4913-4923. https://doi.org/10.1029/2019GL082269

MONDAL AND MISHRA 12 of 12